

The impact of XENON100 and the LHC on Supersymmetric Dark Matter*

Keith A. Olive

William I. Fine Theoretical Physics Institute,
School of Physics and Astronomy, University of Minnesota,
Minneapolis, Minnesota 55455, USA

*To be published in the Proceedings of the 7th DSU Conference, Beijing China

E-mail: olive@umn.edu

Abstract.

The effect of 2010 and 2011 LHC data are discussed in connection to the potential for the direct detection of supersymmetric dark matter. The impact of the recent XENON100 results are contrasted to these predictions.

1. Introduction

The minimal supersymmetric Standard Model (MSSM) has over 100 undetermined parameters, which are mainly associated with the breaking of supersymmetry. However, it is often assumed that the soft supersymmetry-breaking parameters have some universality properties. These may include the universality of gaugino masses, $M_a = m_{1/2}$, trilinear supersymmetry-breaking mass parameters, $A_f = A_0$, and soft scalar masses. $m_{ij}^2 = \delta_{ij}m_0^2$. The simplified version of the MSSM in which universality in input at the grand unification scale is called the constrained MSSM (CMSSM) [1, 2, 3, 4, 5, 6, 7, 8]. The sparticle spectrum is run down to the electroweak scale and radiatively induces electroweak symmetry breaking (EWSB).

Minimization of the Higgs potential leads to two conditions at the weak scale which can be expressed as

$$\mu^2 = \frac{m_1^2 - m_2^2 \tan^2 \beta + \frac{1}{2}m_Z^2(1 - \tan^2 \beta) + \Delta_\mu^{(1)}}{\tan^2 \beta - 1 + \Delta_\mu^{(2)}}, \quad (1)$$

and

$$B\mu = (m_1^2 + m_2^2 + 2\mu^2) \sin 2\beta + \Delta_B \quad (2)$$

where μ is the Higgs mixing parameter, B is the associated supersymmetry-breaking bilinear mass, $\tan \beta$ is the ratio of the two Higgs vacuum expectation values, and Δ_B and $\Delta_\mu^{(1,2)}$ are loop corrections [9, 10, 11]. The combination $B\mu$ can be related to the Higgs pseudo-scalar mass, m_A . While one can choose to include B and μ (or m_A and μ) as free input parameters and calculate the two Higgs expectation values, or m_Z and $\tan \beta$, it is more common to use these equations to calculate μ and B upon assuming a value of $\tan \beta$ and the measured value of m_Z . Thus upon assuming radiative electroweak symmetry breaking, the CMSSM is a 4 parameter theory ($m_{1/2}, m_0, A_0$ and $\tan \beta$). In addition the sign of the μ term must also be specified.

An often considered generalization of the CMSSM allows for non-universal Higgs masses (NUHM) [12, 13, 14]. By allowing, both Higgs soft masses m_1 and m_2 to differ from m_0 (NUHM2), one can effectively choose both m_A and μ as free parameters as is seen from the electroweak conditions given above. One may also choose a subset of these models and take $m_1 = m_2 \neq m_0$ in which case either m_A or μ can be chosen in addition to the four CMSSM parameters (NUHM1).

It is also possible to consider a very constrained version of the MSSM (VCMSSM) [15] by applying the relation $B_0 = A_0 - m_0$ as expected from minimal supergravity [16]. In this case, μ and $\tan\beta$ are derived from the electroweak vacuum conditions and the theory has only three free parameters (and the sign of μ). True models based on minimal supergravity (mSUGRA) impose in addition the relation between the gravitino mass and m_0 , namely $m_{3/2} = m_0$. In these models, it is often the gravitino which ends up as the lightest supersymmetric particle (LSP) and therefore the dark matter candidate.

For given values of $\tan\beta$, A_0 , and $\text{sgn}(\mu)$, the regions of the CMSSM parameter space that yield an acceptable relic density and satisfy other phenomenological constraints may be displayed in the $(m_{1/2}, m_0)$ plane. In Fig. 1a, the dark (blue) shaded region corresponds to that portion of the CMSSM plane with $\tan\beta = 10$, $A_0 = 0$, and $\mu > 0$ such that the computed relic density yields the WMAP value [17] of

$$\Omega h^2 = 0.111 \pm 0.006. \quad (3)$$

The bulk region at relatively low values of $m_{1/2}$ and m_0 , tapers off as $m_{1/2}$ is increased. At higher values of m_0 , annihilation cross sections are too small to maintain an acceptable relic density and $\Omega_\chi h^2$ is too large. At large $m_{1/2}$, co-annihilation processes between the LSP and the next lightest sparticle (in this case the $\tilde{\tau}$) enhance the annihilation cross section and reduce the relic density. This occurs when the LSP and NLSP are nearly degenerate in mass. The dark (red) shaded region has $m_{\tilde{\tau}} < m_\chi$ and is excluded. The effect of coannihilations is to create an allowed band about 25-50 GeV wide in m_0 for $m_{1/2} \lesssim 950$ GeV, or $m_\chi \lesssim 400$ GeV, which tracks above the $m_{\tilde{\tau}_1} = m_\chi$ contour [18]. Also shown in the figure are some phenomenological constraints from the lack of detection of charginos [19], or Higgses [20] as well as constraints from $b \rightarrow s\gamma$ [21] and $g_\mu - 2$ [22]. The locations of these constraints are described in the caption.

At larger $m_{1/2}, m_0$ and $\tan\beta$, the relic neutralino density may be reduced by rapid annihilation through direct-channel H, A Higgs bosons, as seen in Fig. 1(b) [1, 3]. Finally, the relic density can again be brought down into the WMAP range at large m_0 in the ‘focus-point’ region close the boundary where EWSB ceases to be possible and the lightest neutralino χ acquires a significant higgsino component [23]. The start of the focus point region is seen in the upper left of Fig. 1b.

2. Mastercode: Markov-Chain Monte-Carlo

It is well established that Markov-Chain Monte-Carlo (MCMC) algorithms offer an efficient technique for sampling a large parameter space such as the CMSSM or its variants. MCMC has been utilized in the Mastercode [24] framework which incorporates a code for the electroweak observables based on [25] as well as the `SoftSUSY` [26], `FeynHiggs` [27], `SuFla` [28], `SuperIso` [29], `MicrOMEGAs` [30] and `SSARD` [31] codes, using the SUSY Les Houches Accord [32]. The MCMC technique is used to sample the SUSY parameter space, and thereby construct the χ^2 probability function, $P(\chi^2, N_{\text{dof}})$. This accounts for the number of degrees of freedom, N_{dof} , and thus provides a quantitative measure for the quality-of-fit such that $P(\chi^2, N_{\text{dof}})$ can be used to estimate the absolute probability with which the CMSSM describes the experimental data.

The results of the mastercode analysis include the parameters of the best-fit points as well as the 68 and 95% C.L. regions found with default implementations of the phenomenological, experimental and cosmological constraints. These include precision electroweak data, the anomalous magnetic moment of the muon, $(g - 2)_\mu$, B -physics observables, the bound on

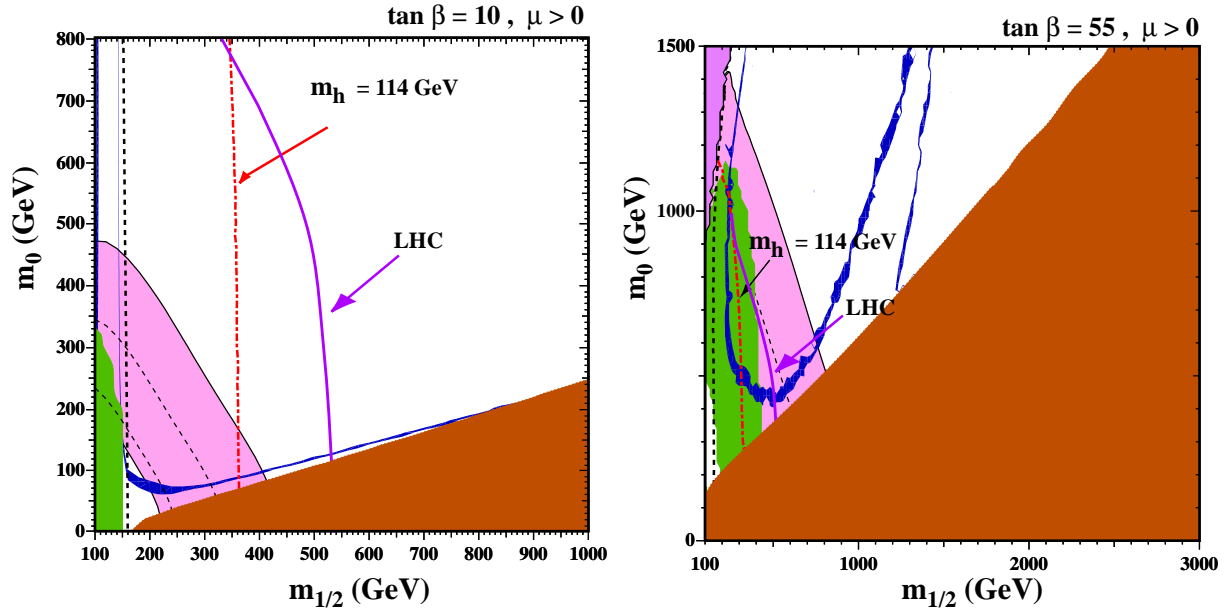


Figure 1. The $(m_{1/2}, m_0)$ planes for (a) $\tan\beta = 10$ and $\mu > 0$, assuming $A_0 = 0, m_t = 173.1$ GeV and $m_b(m_b)_{\overline{MS}}^{SM} = 4.25$ GeV. The near-vertical (red) dot-dashed lines are the contours $m_h = 114$ GeV, and the near-vertical (black) dashed line is the contour $m_{\chi_{\pm}} = 104$ GeV. The medium (dark green) shaded region is excluded by $b \rightarrow s\gamma$, and the dark (blue) shaded area is the cosmologically preferred region. In the dark (brick red) shaded region, the LSP is the charged $\tilde{\tau}_1$. The region allowed by the E821 measurement of $g_\mu - 2$ at the $2\text{-}\sigma$ level, is shaded (pink) and bounded by solid black lines, with dashed lines indicating the $1\text{-}\sigma$ ranges. The curves marked LHC show the 95% CL exclusion region (to the left of the curves) for LHC sparticle searches at $1/\text{fb}$. In (b), $\tan\beta = 55$. Here, in the upper left corner, the region with no EWSB is shaded dark pink.

the lightest MSSM Higgs boson mass, M_h , and the cold dark matter (CDM) density inferred from astrophysical and cosmological data assuming that this is dominated by the relic density of the lightest neutralino, $\Omega_\chi h^2$. In addition one can include the constraint imposed by the experimental upper limit on the spin-independent DM scattering cross section σ_p^{SI} . A purely frequentist analyses of the CMSSM was performed in [6, 7, 8, 33, 34, 35], in the NUHM1 in [8, 33, 34, 35], and in the VCMSSM/mSUGRA in [36, 33, 34].

In [7], a pre-LHC analysis of the CMSSM was performed. The 68% and 95% confidence-level (C.L.) regions in the $(m_{1/2}, m_0)$ plane of the CMSSM are shown in Fig. 2. Also shown for comparison are the physics reaches of ATLAS and CMS with $1/\text{fb}$ of integrated luminosity [37, 38]. The likelihood analysis assumed $\mu > 0$, as motivated by the sign of the apparent discrepancy in $g_\mu - 2$, but sampled all values of $\tan\beta$ and A_0 : the experimental sensitivities were estimated assuming $\tan\beta = 10$ and $A_0 = 0$, but are probably not very sensitive to these assumptions. The global maximum of the likelihood function (indicated by the black dot) is at $m_{1/2} = 310$ GeV, $m_0 = 60$ GeV, $A_0 = 240$ GeV, $\tan\beta = 11$ and $\chi^2/N_{\text{dof}} = 20.4/19$ (37% probability). Note that the best-fit point lies well within the LHC discovery range, as does the 68% C.L. region. As we will see, by the end of 2011, the LHC has met this reach (at 7 TeV center of mass energy) and as sparticles have yet to be discovered, this region is mostly excluded at 95% CL (see sections 4 and 5 below). A more detailed view of the $\Delta\chi^2$ function for the CMSSM is shown in Fig. 3. For other pre-LHC results see [39].

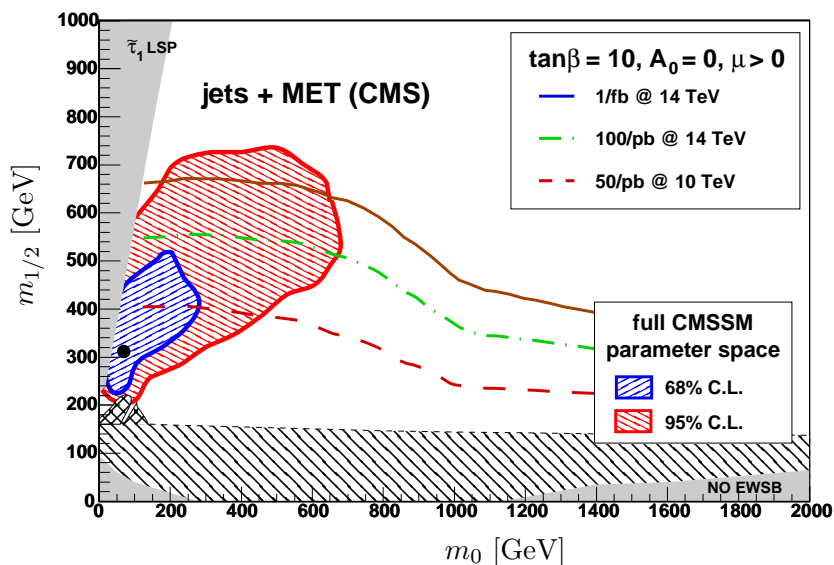


Figure 2. The $(m_0, m_{1/2})$ plane in the CMSSM showing the regions favoured in a likelihood analysis at the 68% (blue) and 95% (red) confidence levels [7]. The best-fit point is shown by the black point. Also shown are the 5σ discovery contours for jet + missing E_T events at CMS with 1 fb^{-1} at 14 TeV, 100 pb^{-1} at 14 TeV and 50 pb^{-1} at 10 TeV centre-of-mass energy.

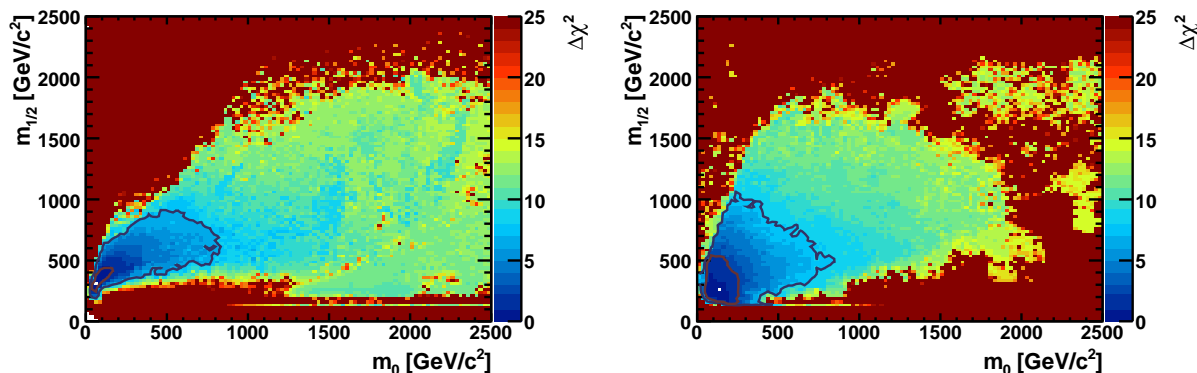


Figure 3. The $\Delta\chi^2$ functions in the $(m_0, m_{1/2})$ planes for the CMSSM (left plot) and for the NUHM1 (right plot). The best fit points are indicated by a white dot and the 68% and 95% CL contours are the light and dark curves respectively [8].

3. Results for the NUHM1

The cosmologically preferred regions move around in the $(m_{1/2}, m_0)$ plane if one abandons the universality assumptions of the CMSSM. As discussed above, if one allows the supersymmetry-breaking contributions to the Higgs masses to be non-universal (NUHM), the rapid-annihilation WMAP ‘strip’ can appear at different values of $\tan\beta$ and $m_{1/2}$, as seen in Fig. 4 [14]. In the left panel, we show an NUHM1 $(m_{1/2}, m_0)$ plane for $\tan\beta = 10$, $A_0 = 0$ and $\mu > 0$ with $m_A = 500$ GeV, and μ calculated using (1). In addition to the constraints discussed above, we also plot contours of $\mu = 300, 500, 1000,$ and 1500 GeV (light pink). The thick green dot-dashed contour tracks the CMSSM parameters in the NUHM1 $(m_{1/2}, m_0)$ plane. The most prominent departure from the CMSSM is that the EWSB requirement constrains the plane at low m_0 rather than at large m_0 . In this region (below the CMSSM contour), the fixed value m_A is larger than its

corresponding value in the CMSSM, resulting in correspondingly larger m_1^2 and m_2^2 (smaller $|m_2^2|$, since $m_2^2 < 0$). We see from (1) that, the effect is to drive μ^2 smaller, and eventually negative. The stau LSP exclusion regions are qualitatively similar to those in the CMSSM, however there is a (black shaded) region of the plane where the lighter selectron is the LSP. In this case, the co-annihilation region connects the analogue of the focus point region with small μ discussed above and heavy Higgs funnel region which now exists at $\tan\beta = 10$ at $m_{1/2} \approx 550$ GeV and extends to large m_0 . Some of the co-annihilation region also extends to larger $m_{1/2}$.

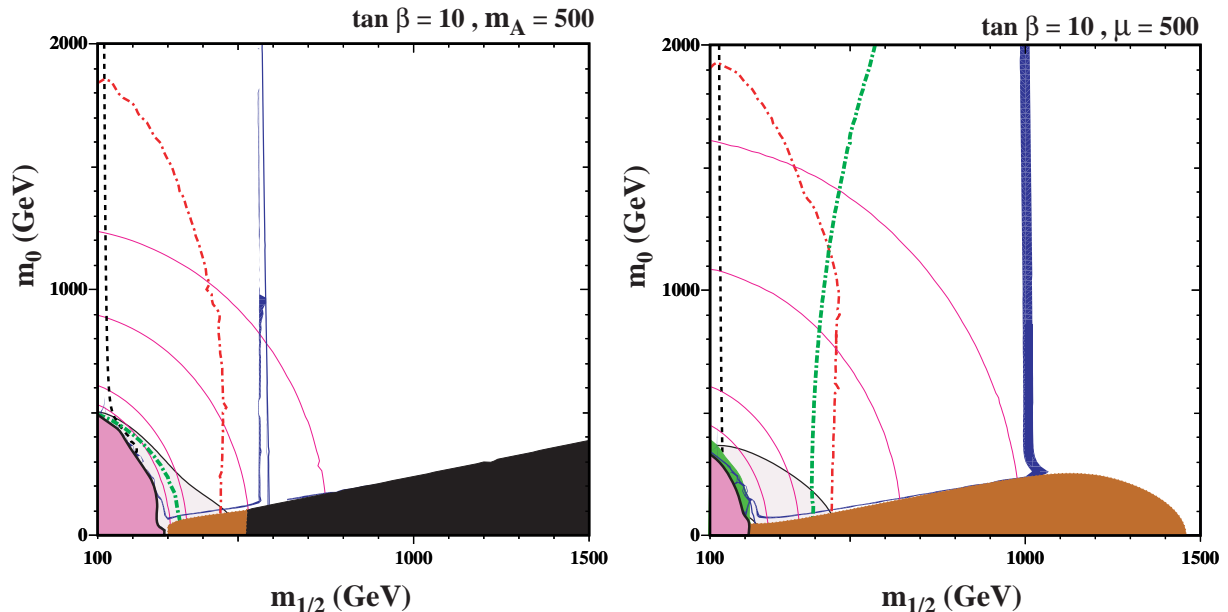


Figure 4. The $(m_{1/2}, m_0)$ plane in the NUHM1 for $\tan\beta = 10$, a) with fixed $m_A = 500$ GeV and b) with fixed $\mu = 500$ GeV [14].

In the right panel of Fig. 4, we show the NUHM1 $(m_{1/2}, m_0)$ plane with $\mu = 500$ GeV and m_A calculated using (2). At first glance, the $(m_{1/2}, m_0)$ plane with fixed μ has some similarities with those with fixed m_A . There are excluded regions at very low $(m_{1/2}, m_0)$ where the pseudoscalar Higgs mass squared is negative, corresponding to the absence of electroweak symmetry breaking, surrounded by four contours of fixed $m_A = 300, 500, 1000,$ and 1500 GeV. At small values of m_0 , extending out to large $m_{1/2}$, there are excluded $\tilde{\tau}$ -LSP regions resembling those in the CMSSM. $b \rightarrow s\gamma$ excludes strips near the EWSB boundary. In addition to the coannihilation strip close to the $\tilde{\tau}$ -LSP boundary, another strip close to the EWSB boundary, and the curved rapid-annihilation funnels that appear at low m_A , with strips of good relic density forming the funnel walls, there is a fourth, near-vertical strip, where the relic density is brought down into the WMAP range because of the large mixing between the bino and Higgsino components in the LSP. For smaller $m_{1/2} < 500$ GeV, the LSP is almost pure bino, and the relic density is too large except in the narrow strips mentioned previously. On the other hand, for larger $m_{1/2} > 1000$ GeV, the LSP is almost pure Higgsino, and the relic density falls below the WMAP range. It is also this change in the nature of the LSP that causes the boundary of the $\tilde{\tau}$ -LSP region to drop. Since the $\tilde{\tau}$ mass is affected only minimally by the value of μ , we find that $\tilde{\tau}$ -LSP region terminates at some value of $m_{1/2}$ related primarily to μ . At large m_0 in panel (b) of Fig. 4, it is only in the ‘crossover’ strip that the relic density falls within the WMAP range. The CMSSM contour is a roughly vertical thick green dot-dashed line, the position of which is determined by the value of m_A that one would find from the electroweak vacuum conditions in

the standard CMSSM.

The results of the Mastercode (pre-LHC) analysis for the NUHM1 is shown in the right panel of Fig. 3. The corresponding parameters of the best-fit NUHM1 point are $m_0 = 150$ GeV, $m_{1/2} = 270$ GeV, $A_0 = -1300$ GeV, $\tan\beta = 11$ and $m_{h_1}^2 = m_{h_2}^2 = -1.2 \times 10^6$ GeV² or, equivalently, $\mu = 1140$ GeV, yielding $\chi^2 = 18.4$ (corresponding to a similar fit probability to the CMSSM) and $M_h = 120.7$ GeV.

It is also possible to extract 1D likelihood functions for essentially any parameter of interest. Here, we show in Fig. 5 the $\Delta\chi^2$ function for the lightest neutralino mass in both the CMSSM and NUHM1. The left panel of Fig. 5 displays the likelihood function in the CMSSM. The solid line shows the result obtained when incorporating the LEP Higgs limit, while the dashed line corresponds to the case where the LEP Higgs constraint is removed. There is a sharp rise in the likelihood function at low values of $m_{\tilde{\chi}_1^0}$, which is caused by the limits from the direct searches for SUSY particles, but receives also contributions from $\text{BR}(b \rightarrow s\gamma)$ and other constraints. This sharp rise in the likelihood function persists when the LEP Higgs constraint is removed, but is shifted towards slightly lower values of $m_{\tilde{\chi}_1^0}$ in that case. The right panel of Fig. 5 shows the likelihood function for $m_{\tilde{\chi}_1^0}$ in the NUHM1, again with and without the LEP M_h constraint imposed.

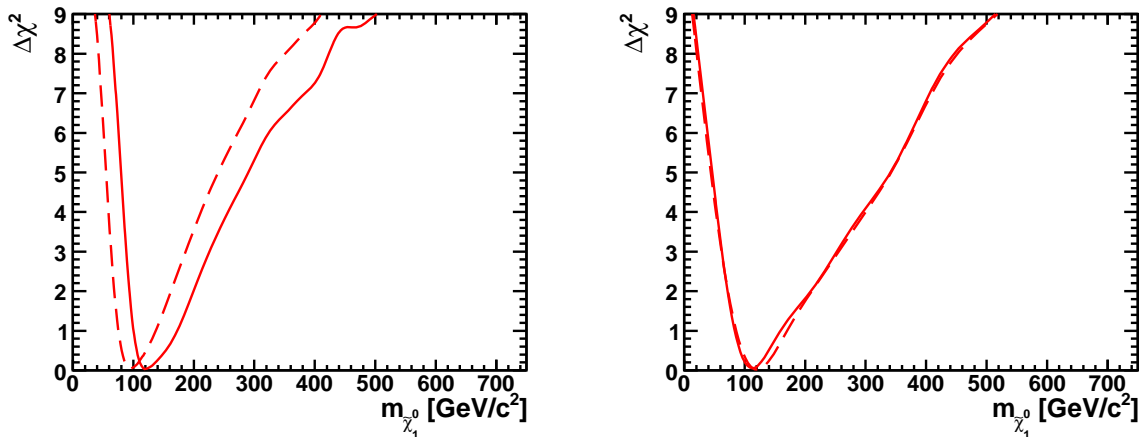


Figure 5. The likelihood functions for $m_{\tilde{\chi}_1^0}$ in the CMSSM (left) and in the NUHM1 (right), both with (solid lines) and without (dashed lines) the LEP constraint on M_h [8].

4. Early Results from the LHC

As 2010 came to a close, we obtained the first results from the LHC on sparticle searches. These include several new constraints on SUSY using an integrated luminosity of $\sim 35/\text{pb}$ of data at 7 TeV. ATLAS has published the results of a search in multijet + \cancel{E}_T channels (ATLAS 0L) [40] that has greater sensitivity in some regions to the types of gluino and squark pair-production events expected in the supersymmetric models discussed here than did the earlier ATLAS 1L search [41], and has also released results obtained by combining the one- and zero-lepton searches [42]. CMS has announced results from two other searches in multijet + \cancel{E}_T channels that improve the CMS α_T sensitivity also to gluino and squark production in the models discussed here [43, 44].

In addition, the XENON100 Collaboration has recently released results from a search for direct spin-independent dark matter scattering with 100.9 live days of data using a fiducial

target with a mass of 48 kg [45]. As we see later, this provides constraints on the parameter spaces of supersymmetric models that complement those provided by collider experiments.

The impact of the 35/pb LHC data on the CMSSM parameter space is rather dramatic [33, 34, 35] (see also [46]). In Fig. 6, we display the planes for the CMSSM (left) and NUHM1 (right) driven by the ATLAS 0L and CMS MHT constraints but also taking into account the other 2010 LHC constraints, as well as the XENON100 constraint [34]. The best-fit points are shown as green stars and 68 and 95% CL regions are shown as red and blue lines, respectively and correspond to $\Delta\chi^2 = 2.3$ (red) and 5.99 (blue) relative to the best fit points. The pre-LHC results, taken from [33], are displayed as ‘snowflakes’ and dotted lines, the post-2010-LHC/XENON100 results are displayed as full stars and solid lines [34].

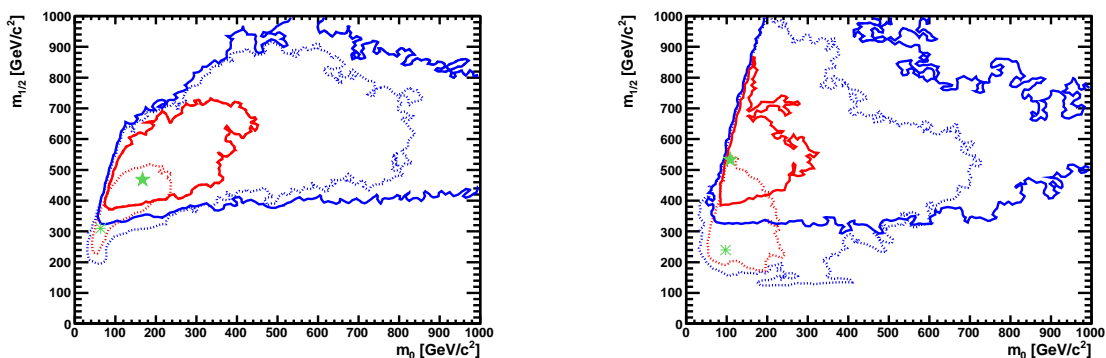


Figure 6. The $(m_0, m_{1/2})$ planes in the CMSSM (left), and the NUHM1 (right). In each plane, the best-fit point after incorporation of the 2010 LHC and XENON100 constraints is indicated by a filled green star, and the pre-LHC fit by an open star. The 68 and 95% CL regions are indicated by red and blue contours, respectively, the solid lines including the 2010 LHC and XENON100 data, and the dotted lines showing the pre-LHC fits [33, 34].

In the CMSSM and the NUHM, the direct 2010 LHC constraints push the best-fit values of $m_{1/2}$ to significantly higher values, as well as their 68 and 95% CL ranges. The effect of the LHC on the best-fit values of m_0 is smaller, though there is a significant increase in the CMSSM that is correlated with the increase in $m_{1/2}$. The positions of the best fit points pre/post LHC are collected in Table 1. The total value of χ^2 and the number of degrees of freedom (dof) along with the fit probably (p-value) are also given. The final column shows the predicted value of the Higgs mass at the best fit point. Note there is a slight shift in the best fit points for the pre-LHC data due to changes in the input data used in the Mastercode analysis. LHC2010 includes the 35/pb LHC data as well as the XENON100 data. While one would expect two additional dof’s, one dof (the Higgs mass constraint) is lost since the best fit point is pushed past the previous LEP sensitivity.

5. The LHC @ 1/fb

By mid 2011, the LHC results for sparticle searches based on 1/fb of analyzed data were released by the ATLAS [47, 48], CMS [49, 50, 51] and LHCb Collaborations [52]. The absences of signals in the jets + \cancel{E}_T searches disfavour the ranges of the model mass parameters $(m_0, m_{1/2})$ that had been favoured in our previous analyses of the CMSSM and NUHM1 [33, 34], and our current best fits have $m_0 \sim 150$ to 450 GeV and $m_{1/2} \sim 750$ GeV. Reconciling these larger values of $(m_0, m_{1/2})$ with $(g-2)_\mu$ favours values of $\tan\beta \sim 40$, though with a large uncertainty. Fig. 7 shows the positions of the 68 and 95% CL contours with solid curves corresponding to the 1/fb data as compared with the pre-LHC (and pre-XENON100) results (dashed) [35].

Model	Minimum $\chi^2/\text{d.o.f.}$	Prob- ability	$m_{1/2}$ (GeV)	m_0 (GeV)	A_0 (GeV)	$\tan\beta$	M_h (GeV) (no LEP)
CMSSM pre-LHC	21.5/20	37%	360	90	-400	15	111.5
LHC 2010	25.2/21	24%	470	170	-780	22	115.7
LHC _{1/fb}	28.8/22	15%	780	450	-1100	41	119.1
$(g-2)_\mu$ neglected	21.3/20	38%	2000	1050	430	22	124.8
NUHM1 pre-LHC	20.8/18	29%	340	110	520	13	118.9
LHC 2010	24.5/20	22%	530	110	-370	27	117.9
LHC _{1/fb}	27.3/21	16%	730	150	-910	41	118.8
$(g-2)_\mu$ neglected	20.3/19	38%	2020	1410	2580	48	126.6

Table 1. Comparison of the best-fit points found in the CMSSM and NUHM1 pre-LHC (including the upper limit on $BR(B_s \rightarrow \mu^+ \mu^-)$ available then), the LHC 2010 result (including XENON100) and with the LHC_{1/fb} data set (also including the XENON100 constraint) using the standard implementations of the $(g-2)_\mu$ constraint, followed by the case dropping $(g-2)_\mu$. The predictions for M_h do not include the constraint from the direct LEP Higgs search.

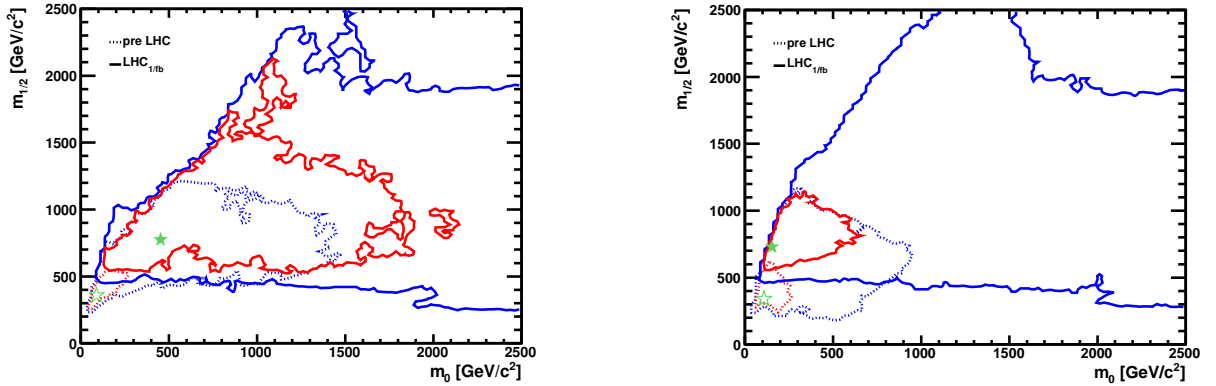


Figure 7. The $(m_0, m_{1/2})$ planes in the CMSSM (left) and the NUHM1 (right). In each plane, the best-fit point after incorporation of the LHC_{1/fb} constraints is indicated by a filled green star, and the pre-LHC fit [36] by an open star. The 68 and 95% CL regions are indicated in red and blue, respectively, the solid lines including the LHC_{1/fb} data and the dotted lines showing the pre-LHC fits [35].

The positions of the best fit points at 1/fb are tabulated in Table 1. We now find that the p -value for the CMSSM best-fit point is now $\sim 15\%$, and that for the NUHM1 is $\sim 16\%$. On the other hand, if the $(g-2)_\mu$ constraint is dropped much larger regions of the $(m_0, m_{1/2})$ and other parameter planes are allowed at the 68 and 95% CL, and these p -values increase to 38% in both models. For comparison, the p -value for the Standard Model (including $(g-2)_\mu$) is 9%.

In Fig. 8 we show the 68% and 95% CL contours in the $(m_{\tilde{\chi}_1^0}, \sigma_p^{\text{SI}})$ planes for the CMSSM (left) and the NUHM1 (right). The solid lines are based on our global fits including the LHC_{1/fb} constraints, whereas the dotted lines correspond to our previous fits using the pre-

LHC constraints. In both cases, we assume $\Sigma_{\pi N} = 50 \pm 14$ MeV [53]¹, and we include with the $\text{LHC}_{1/\text{fb}}$ data the XENON100 constraint on σ_p^{SI} [45]. We see that the $\text{LHC}_{1/\text{fb}}$ data tend to push $m_{\tilde{\chi}_1^0}$ to larger values, and that these are correlated with lower values of σ_p^{SI} , though with best-fit values still $\sim 10^{-45}$ cm² [35].

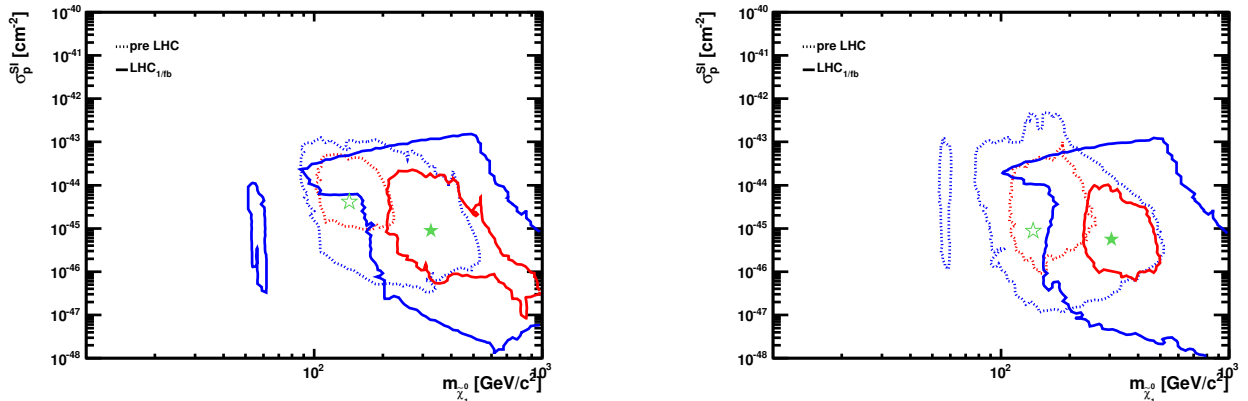


Figure 8. The 68% and 95% CL contours (red and blue, respectively) in the CMSSM (left) and the NUHM1 (right). The solid lines are for fits including the XENON100 [45] and $\text{LHC}_{1/\text{fb}}$ data, whereas the dotted lines include only the pre-LHC data [35].

6. The Higgs Search

At the close of 2011, the ATLAS and CMS Collaborations have released their official combination of the searches for a SM Higgs boson with the first $\sim 1 - 2.3/\text{fb}$ of LHC luminosity at $E_{\text{cm}} = 7$ TeV [54]. The combination excludes a SM Higgs boson with a mass between 141 and 476 GeV. Additionally, the ATLAS and CMS Collaborations have presented preliminary updates of their results with $\sim 5/\text{fb}$ of data [55]. These results may be compatible with a SM-like Higgs boson around $M_h \simeq 125$ GeV, though CMS also report an excess at $M_h \simeq 119$ GeV in the ZZ^* channel.

It is interesting to note that based on the LHC 1/fb results, we have the predictions of the Higgs mass as seen in Table 1 of 119 and 125 GeV depending on whether $(g - 2)_\mu$ is included in the analysis [35]. Specifically, the 1/fb fits included $M_h = 119.1^{+3.4}_{-2.9}$ GeV in the CMSSM and $M_h = 118.8^{+2.7}_{-1.1}$ GeV in the NUHM1 (which should be combined with an estimated theory error $\Delta M_h = \pm 1.5$ GeV). These two fits are based solely on the Higgs-independent searches including the $(g - 2)_\mu$ constraint, i.e., they do not rely on the existing limits from LEP [20, 56], the Tevatron [57], or the LHC [48, 50]. These predictions increase to $M_h = 124.8^{+3.4}_{-10.5}$ GeV in the CMSSM and $126.6^{+0.7}_{-1.9}$ GeV in the NUHM1 if the $(g - 2)_\mu$ constraint is dropped.

If indeed, the LHC has seen the Higgs at 125 ± 1 (119 \pm 1) GeV, there are rather dramatic consequences for the supersymmetric parameter space [58] (see also [59]). Since in the CMSSM and NUHM1 the radiative corrections contributing to the value of M_h are sensitive primarily to $m_{1/2}$ and $\tan \beta$, and only to a lesser extent to m_0 , we expect that the primary effect of imposing the M_h constraint should be to affect the preferred ranges of $m_{1/2}$ and $\tan \beta$, with a lesser effect on the preferred range of m_0 . This effect is indeed seen in both panels of Fig. 9. We see that the 68% CL ranges of $m_{1/2}$ extend to somewhat larger values and with a wider spread than the pre-Higgs results, particularly in the NUHM1. However, the NUHM1 best-fit value of

¹ We recall the sensitivity of predictions for σ_p^{SI} to the uncertainty in $\Sigma_{\pi N}$ [34].

$m_{1/2}$ remains at a relatively low value of ~ 800 GeV, whereas the best-fit value of $m_{1/2}$ in the CMSSM moves to ~ 1900 GeV. This jump reflects the flatness of the likelihood function for $m_{1/2}$ between ~ 700 GeV and ~ 2 TeV.

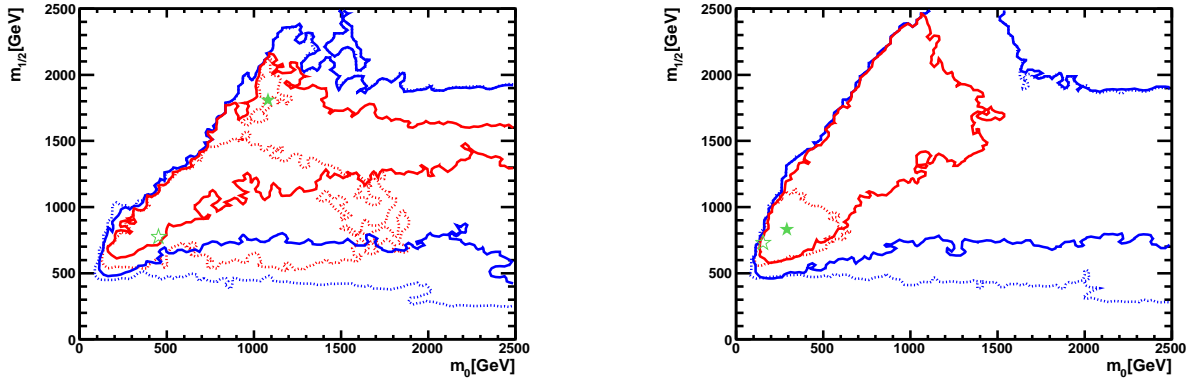


Figure 9. The $(m_0, m_{1/2})$ planes in the CMSSM (left) and the NUHM1 (right). The 68 and 95% CL regions are indicated in red and blue, respectively, the solid lines including the hypothetical LHC measurement $M_h = 125 \pm 1$ GeV and allowing for a theoretical error ± 1.5 GeV [58], and the dotted lines showing the contours found previously in [35] without this M_h constraint. Here the open green stars denote the pre-Higgs best-fit points, whereas the solid green stars indicate the new best-fit points.

In Fig. 10 we show results for the preferred regions in the $(m_{\tilde{\chi}_1^0}, \sigma_p^{\text{SI}})$ plane. As seen in Fig. 10, the fact that larger values of $m_{1/2}$ and hence $m_{\tilde{\chi}_1^0}$ are favoured by the larger values of M_h implies that at the 68% CL the preferred range of σ_p^{SI} is significantly lower when $M_h \simeq 125$ GeV, when compared to our previous best fit with $M_h = 119$ GeV, rendering direct detection of dark matter significantly more difficult. Again, this effect on $m_{\tilde{\chi}_1^0}$ is more pronounced in the CMSSM, whereas in the NUHM1 the value of $m_{\tilde{\chi}_1^0}$ for the best-fit point changes only slightly.

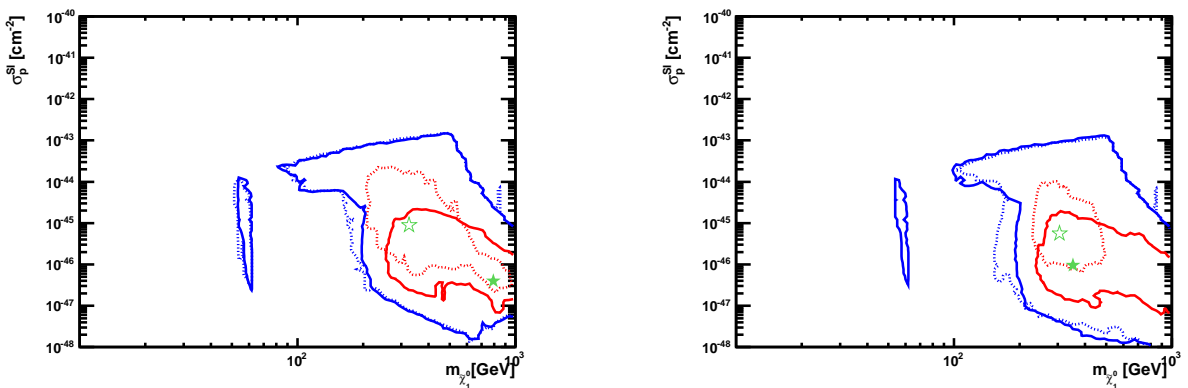


Figure 10. The $(m_{\tilde{\chi}_1^0}, \sigma_p^{\text{SI}})$ planes in the CMSSM (left) and the NUHM1 (right), for $M_h \simeq 125$ GeV. The notations and significations of the contours are the same as in Fig. 8 [58].

If instead, we assume an alternative potential LHC measurement $M_h = 119 \pm 1$ GeV, which corresponds to the CMS ZZ^* signal and our earlier predictions including the $(g-2)_\mu$ constraint,

we obtain the $(m_0, m_{1/2})$ planes shown in Fig. 11. Since this assumed LHC value of M_h coincides with the previous best-fit values in both the CMSSM and NUHM1, the best-fit points in these models (indicated by the green stars in Fig. 11) are unaffected by the imposition of the putative LHC constraint. The effect of the hypothetical measurement restricting the range in $m_{1/2}$ is indeed seen in both panels of Fig. 11, though for the 68% CL contour (shown in red) it is much more pronounced for the CMSSM than for the NUHM1.

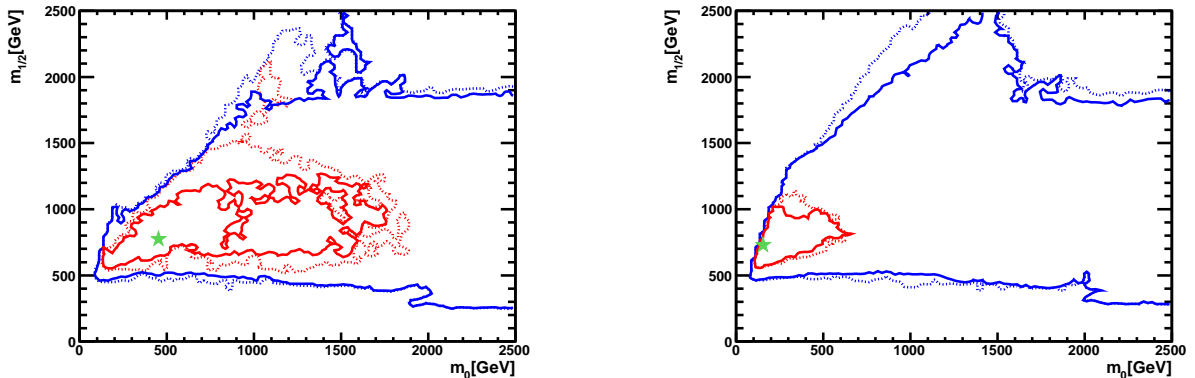


Figure 11. The $(m_0, m_{1/2})$ planes in the CMSSM (left) and the NUHM1 (right) assuming a hypothetical measurement of $M_h = 119 \pm 1$ GeV. The notations and significations of the contours are the same as in Fig. 7 [58].

In this case, in both the CMSSM and the NUHM1 there is little impact on the 95% CL regions nor on the 68% CL region in the NUHM1 in the (m_χ, σ_p^{SI}) plane. The only substantial change, as can be seen in Fig. 12, appears in the 68% CL region of the CMSSM, where now values of $m_{\tilde{\chi}_1^0} \gtrsim 500$ GeV and $\sigma_p^{SI} 10^{-46} \text{ cm}^2$ are disfavoured after the inclusion of a Higgs-boson mass measurement at 119 GeV.

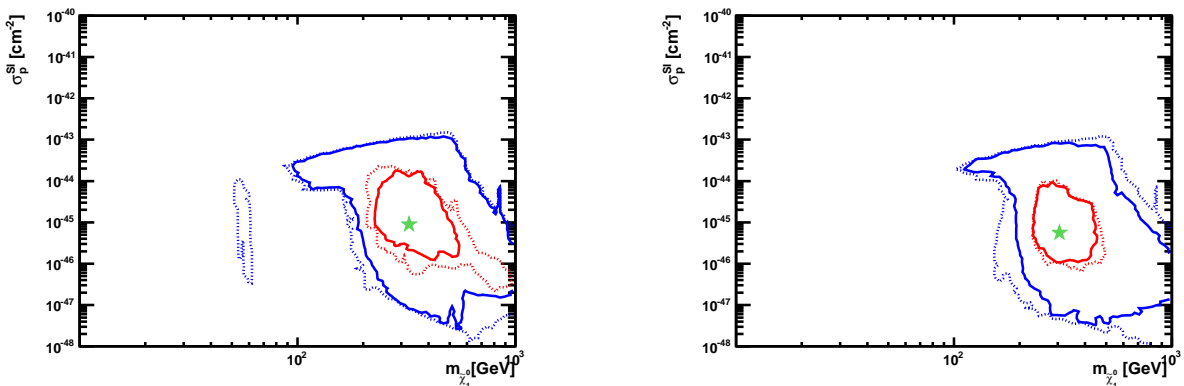


Figure 12. The $(m_{\tilde{\chi}_1^0}, \sigma_p^{SI})$ planes in the CMSSM (left) and the NUHM1 (right), for $M_h \simeq 119$ GeV. The notations and significations of the contours are the same as in Fig. 11 [58].

The past year has shown an immense amount of activity. We have seen direct detection experiments (XENON100 [45]) for the first time have a direct impact on supersymmetric parameter space making these data a necessary input to a global likelihood analysis. The

LHC constraints have moved at a frightening pace. As reviewed here, starting with the 35/pb data, our notion of the best fit point in the CMSSM and indeed our prospects for low energy supersymmetry are greatly different as we start 2012 compared with the pre-LHC era.

Acknowledgments

I would like to thank all the members of Mastercode collaboration whose work went into the summary presented here. This work was supported in part by DOE grant DE-FG02-94ER-40823 at the University of Minnesota.

References

- [1] M. Drees and M. M. Nojiri, *Phys. Rev. D* **47** (1993) 376 [arXiv:hep-ph/9207234]; H. Baer and M. Brhlik, *Phys. Rev. D* **53** (1996) 597 [arXiv:hep-ph/9508321]; *Phys. Rev. D* **57** (1998) 567 [arXiv:hep-ph/9706509]; H. Baer, M. Brhlik, M. A. Diaz, J. Ferrandis, P. Mercadante, P. Quintana and X. Tata, *Phys. Rev. D* **63** (2001) 015007 [arXiv:hep-ph/0005027].
- [2] G. L. Kane, C. F. Kolda, L. Roszkowski and J. D. Wells, *Phys. Rev. D* **49** (1994) 6173 [arXiv:hep-ph/9312272]; J. R. Ellis, T. Falk, K. A. Olive and M. Schmitt, *Phys. Lett. B* **388** (1996) 97 [arXiv:hep-ph/9607292]; *Phys. Lett. B* **413** (1997) 355 [arXiv:hep-ph/9705444]; J. R. Ellis, T. Falk, G. Ganis, K. A. Olive and M. Schmitt, *Phys. Rev. D* **58** (1998) 095002 [arXiv:hep-ph/9801445]; V. D. Barger and C. Kao, *Phys. Rev. D* **57** (1998) 3131 [arXiv:hep-ph/9704403]; J. R. Ellis, T. Falk, G. Ganis and K. A. Olive, *Phys. Rev. D* **62** (2000) 075010 [arXiv:hep-ph/0004169].
- [3] J. R. Ellis, T. Falk, G. Ganis, K. A. Olive and M. Srednicki, *Phys. Lett. B* **510** (2001) 236 [arXiv:hep-ph/0102098].
- [4] V. D. Barger and C. Kao, *Phys. Lett. B* **518** (2001) 117 [arXiv:hep-ph/0106189]; L. Roszkowski, R. Ruiz de Austri and T. Nihei, *JHEP* **0108** (2001) 024 [arXiv:hep-ph/0106334]; A. Djouadi, M. Drees and J. L. Kneur, *JHEP* **0108** (2001) 055 [arXiv:hep-ph/0107316]; U. Chattopadhyay, A. Corsetti and P. Nath, *Phys. Rev. D* **66** (2002) 035003 [arXiv:hep-ph/0201001]; J. R. Ellis, K. A. Olive and Y. Santoso, *New Jour. Phys.* **4** (2002) 32 [arXiv:hep-ph/0202110]; H. Baer, C. Balazs, A. Belyaev, J. K. Mizukoshi, X. Tata and Y. Wang, *JHEP* **0207** (2002) 050 [arXiv:hep-ph/0205325]; R. Arnowitt and B. Dutta, arXiv:hep-ph/0211417.
- [5] J. R. Ellis, K. A. Olive, Y. Santoso and V. C. Spanos, *Phys. Lett. B* **565** (2003) 176 [arXiv:hep-ph/0303043]; H. Baer and C. Balazs, *JCAP* **0305**, 006 (2003) [arXiv:hep-ph/0303114]; A. B. Lahanas and D. V. Nanopoulos, *Phys. Lett. B* **568**, 55 (2003) [arXiv:hep-ph/0303130]; U. Chattopadhyay, A. Corsetti and P. Nath, *Phys. Rev. D* **68**, 035005 (2003) [arXiv:hep-ph/0303201]; C. Munoz, *Int. J. Mod. Phys. A* **19**, 3093 (2004) [arXiv:hep-ph/0309346]; R. Arnowitt, B. Dutta and B. Hu, arXiv:hep-ph/0310103. J. Ellis and K. A. Olive, arXiv:1001.3651 [astro-ph.CO].
- [6] O. Buchmueller *et al.*, *Phys. Lett. B* **657** (2007) 87 [arXiv:0707.3447 [hep-ph]].
- [7] O. Buchmueller *et al.*, *JHEP* **0809** (2008) 117 [arXiv:0808.4128 [hep-ph]].
- [8] O. Buchmueller *et al.*, *Eur. Phys. J. C* **64** (2009) 391 [arXiv:0907.5568 [hep-ph]].
- [9] V. D. Barger, M. S. Berger and P. Ohmann, *Phys. Rev. D* **49** (1994) 4908 [arXiv:hep-ph/9311269].
- [10] W. de Boer, R. Ehret and D. I. Kazakov, *Z. Phys. C* **67** (1995) 647 [arXiv:hep-ph/9405342].
- [11] M. Carena, J. R. Ellis, A. Pilaftsis and C. E. Wagner, *Nucl. Phys. B* **625** (2002) 345 [arXiv:hep-ph/0111245].
- [12] J. Ellis, K. Olive and Y. Santoso, *Phys. Lett. B* **539**, 107 (2002) [arXiv:hep-ph/0204192]; J. R. Ellis, T. Falk, K. A. Olive and Y. Santoso, *Nucl. Phys. B* **652**, 259 (2003) [arXiv:hep-ph/0210205].
- [13] H. Baer, A. Mustafayev, S. Profumo, A. Belyaev and X. Tata, *Phys. Rev. D* **71**, 095008 (2005) [arXiv:hep-ph/0412059]; H. Baer, A. Mustafayev, S. Profumo, A. Belyaev and X. Tata, *JHEP* **0507** (2005) 065, hep-ph/0504001.
- [14] J. R. Ellis, K. A. Olive and P. Sandick, *Phys. Rev. D* **78**, 075012 (2008) [arXiv:0805.2343 [hep-ph]].
- [15] J. R. Ellis, K. A. Olive, Y. Santoso and V. C. Spanos, *Phys. Lett. B* **573** (2003) 162 [arXiv:hep-ph/0305212], and *Phys. Rev. D* **70** (2004) 055005 [arXiv:hep-ph/0405110].
- [16] J. Polonyi, *Generalization Of The Massive Scalar Multiplet Coupling To The Supergravity*, Hungary Central Inst Res - KFKI-77-93; E. Cremmer, B. Julia, J. Scherk, P. van Nieuwenhuizen, S. Ferrara and L. Girardello, *Phys. Lett. B* **79**, 231 (1978); E. Cremmer, B. Julia, J. Scherk, S. Ferrara, L. Girardello and P. van Nieuwenhuizen, *Nucl. Phys. B* **147**, 105 (1979); R. Barbieri, S. Ferrara and C. A. Savoy, *Phys. Lett. B* **119**, 343 (1982); A. H. Chamseddine, R. L. Arnowitt and P. Nath, *Phys. Rev. Lett.* **49**, 970 (1982).
- [17] E. Komatsu *et al.* [WMAP Collaboration], *Astrophys. J. Suppl.* **192** (2011) 18 [arXiv:1001.4538 [astro-ph.CO]].
- [18] J. Ellis, T. Falk, and K.A. Olive, *Phys. Lett. B* **444** (1998) 367 [arXiv:hep-ph/9810360]; J. Ellis, T.

- Falk, K.A. Olive, and M. Srednicki, *Astr. Part. Phys.* **13** (2000) 181 [Erratum-ibid. **15** (2001) 413] [arXiv:hep-ph/9905481].
- [19] Joint LEP 2 Supersymmetry Working Group, *Combined LEP Chargino Results, up to 208 GeV*, http://lepsusy.web.cern.ch/lepsusy/www/inos_moriond01/charginos_pub.html.
- [20] R. Barate *et al.* [ALEPH, DELPHI, L3, OPAL Collaborations: the LEP Working Group for Higgs boson searches], *Phys. Lett. B* **565**, 61 (2003) [arXiv:hep-ex/0306033]; D. Zer-Zion, *Prepared for 32nd International Conference on High-Energy Physics (ICHEP 04), Beijing, China, 16-22 Aug 2004*; LHWG-NOTE-2004-01, ALEPH-2004-008, DELPHI-2004-042, L3-NOTE-2820, OPAL-TN-744, http://lephiggs.web.cern.ch/LEPHIGGS/papers/August2004_MSSM/index.html.
- [21] S. Chen *et al.* [CLEO Collaboration], *Phys. Rev. Lett.* **87** (2001) 251807 [arXiv:hep-ex/0108032]; P. Koppenburg *et al.* [Belle Collaboration], *Phys. Rev. Lett.* **93** (2004) 061803 [arXiv:hep-ex/0403004]. B. Aubert *et al.* [BaBar Collaboration], arXiv:hep-ex/0207076; E. Barberio *et al.* [Heavy Flavor Averaging Group (HFAG)], arXiv:hep-ex/0603003.
- [22] [The Muon g-2 Collaboration], *Phys. Rev. Lett.* **92** (2004) 161802, hep-ex/0401008; G. Bennett *et al.* [The Muon g-2 Collaboration], *Phys. Rev. D* **73** (2006) 072003 [arXiv:hep-ex/0602035].
- [23] J. L. Feng, K. T. Matchev and T. Moroi, *Phys. Rev. D* **61** (2000) 075005 [arXiv:hep-ph/9909334].
- [24] For more information and updates, please see <http://cern.ch/mastercode/>.
- [25] S. Heinemeyer *et al.*, *JHEP* **0608** (2006) 052 [arXiv:hep-ph/0604147]; S. Heinemeyer, W. Hollik, A. M. Weber and G. Weiglein, *JHEP* **0804** (2008) 039 [arXiv:0710.2972 [hep-ph]].
- [26] B. C. Allanach, *Comput. Phys. Commun.* **143** (2002) 305 [arXiv:hep-ph/0104145].
- [27] G. Degrandi, S. Heinemeyer, W. Hollik, P. Slavich and G. Weiglein, *Eur. Phys. J. C* **28** (2003) 133 [arXiv:hep-ph/0212020]; S. Heinemeyer, W. Hollik and G. Weiglein, *Eur. Phys. J. C* **9** (1999) 343 [arXiv:hep-ph/9812472]; S. Heinemeyer, W. Hollik and G. Weiglein, *Comput. Phys. Commun.* **124** (2000) 76 [arXiv:hep-ph/9812320]; M. Frank *et al.*, *JHEP* **0702** (2007) 047 [arXiv:hep-ph/0611326]; See <http://www.feynhiggs.de>.
- [28] G. Isidori and P. Paradisi, *Phys. Lett. B* **639** (2006) 499 [arXiv:hep-ph/0605012]; G. Isidori, F. Mescia, P. Paradisi and D. Temes, *Phys. Rev. D* **75** (2007) 115019 [arXiv:hep-ph/0703035], and references therein.
- [29] F. Mahmoudi, *Comput. Phys. Commun.* **178** (2008) 745 [arXiv:0710.2067 [hep-ph]]; *Comput. Phys. Commun.* **180** (2009) 1579 [arXiv:0808.3144 [hep-ph]]; D. Eriksson, F. Mahmoudi and O. Stal, *JHEP* **0811** (2008) 035 [arXiv:0808.3551 [hep-ph]].
- [30] G. Belanger, F. Boudjema, A. Pukhov and A. Semenov, *Comput. Phys. Commun.* **176** (2007) 367 [arXiv:hep-ph/0607059]; *Comput. Phys. Commun.* **149** (2002) 103 [arXiv:hep-ph/0112278]; *Comput. Phys. Commun.* **174** (2006) 577 [arXiv:hep-ph/0405253].
- [31] Information about this code is available from K. A. Olive: it contains important contributions from T. Falk, A. Ferstl, G. Gani, A. Mustafayev, J. McDonald, K. A. Olive, P. Sandick, Y. Santoso and M. Srednicki.
- [32] P. Skands *et al.*, *JHEP* **0407** (2004) 036 [arXiv:hep-ph/0311123]; B. Allanach *et al.*, *Comput. Phys. Commun.* **180** (2009) 8 [arXiv:0801.0045 [hep-ph]].
- [33] O. Buchmueller *et al.*, *Eur. Phys. J. C* **71** (2011) 1634 [arXiv:1102.4585 [hep-ph]].
- [34] O. Buchmueller *et al.*, *Eur. Phys. J. C* **71** (2011) 1722 [arXiv:1106.2529 [hep-ph]].
- [35] O. Buchmueller, R. Cavanaugh, A. De Roeck, M. J. Dolan, J. R. Ellis, H. Flacher, S. Heinemeyer and G. Isidori *et al.*, arXiv:1110.3568 [hep-ph].
- [36] O. Buchmueller *et al.*, *Eur. Phys. J. C* **71** (2011) 1583 [arXiv:1011.6118 [hep-ph]].
- [37] "ATLAS detector and physics performance. Technical design report. Vol. 2," , CER-LHCC-99-15.
- [38] G. L. Bayatian *et al.* [CMS Collaboration], *J. Phys. G* **34**, 995 (2007).
- [39] For a sampling of other pre-LHC analyses, see: E. A. Baltz and P. Gondolo, *JHEP* **0410** (2004) 052 [arXiv:hep-ph/0407039]; B. C. Allanach and C. G. Lester, *Phys. Rev. D* **73** (2006) 015013 [arXiv:hep-ph/0507283]; R. R. de Austri, R. Trotta and L. Roszkowski, *JHEP* **0605** (2006) 002 [arXiv:hep-ph/0602028]; R. Lafaye, T. Plehn, M. Rauch and D. Zerwas, *Eur. Phys. J. C* **54** (2008) 617 [arXiv:0709.3985 [hep-ph]]; S. Heinemeyer, X. Miao, S. Su and G. Weiglein, *JHEP* **0808** (2008) 087 [arXiv:0805.2359 [hep-ph]]; R. Trotta, F. Feroz, M. P. Hobson, L. Roszkowski and R. Ruiz de Austri, *JHEP* **0812** (2008) 024 [arXiv:0809.3792 [hep-ph]]; P. Bechtle, K. Desch, M. Uhlenbrock and P. Wienemann, *Eur. Phys. J. C* **66** (2010) 215 [arXiv:0907.2589 [hep-ph]].
- [40] G. Aad *et al.* [Atlas Collaboration], *Phys. Lett. B* **701**, 186 (2011) [arXiv:1102.5290 [hep-ex]].
- [41] G. Aad *et al.* [Atlas Collaboration], *Phys. Rev. Lett.* **106**, 131802 (2011) [arXiv:1102.2357 [hep-ex]].
- [42] G. Aad *et al.* [ATLAS Collaboration], <http://cdsweb.cern.ch/record/1345745/files/ATLAS-CONF-2011-064.pdf>.
- [43] V. Khachatryan *et al.* [CMS Collaboration], *Phys. Lett. B* **698**, 196 (2011) [arXiv:1101.1628 [hep-ex]].
- [44] V. Khachatryan *et al.* [CMS Collaboration], <http://cdsweb.cern.ch/record/1343076/files/SUS-10-005-pas.pdf>; see also

<https://twiki.cern.ch/twiki/bin/view/CMSPublic/PhysicsResultsSUS>.

- [45] E. Aprile *et al.* [XENON100 Collaboration], Phys. Rev. Lett. **107**, 131302 (2011) [arXiv:1104.2549 [astro-ph.CO]].
- [46] D. Feldman, K. Freese, P. Nath, B. D. Nelson and G. Peim, Phys. Rev. D **84**, 015007 (2011) [arXiv:1102.2548 [hep-ph]]; B. C. Allanach, Phys. Rev. D **83**, 095019 (2011) [arXiv:1102.3149 [hep-ph]]; S. Scopel, S. Choi, N. Fornengo and A. Bottino, Phys. Rev. D **83**, 095016 (2011) [arXiv:1102.4033 [hep-ph]]; P. Bechtle *et al.*, arXiv:1102.4693 [hep-ph]; B. C. Allanach, T. J. Khoo, C. G. Lester and S. L. Williams, JHEP **1106**, 035 (2011) [arXiv:1103.0969 [hep-ph]]; S. Akula, N. Chen, D. Feldman, M. Liu, Z. Liu, P. Nath and G. Peim, Phys. Lett. B **699**, 377 (2011) [arXiv:1103.1197 [hep-ph]]; M. J. Dolan, D. Grellscheid, J. Jaeckel, V. V. Khoze and P. Richardson, JHEP **1106**, 095 (2011) [arXiv:1104.0585 [hep-ph]]; S. Akula, D. Feldman, Z. Liu, P. Nath and G. Peim, Mod. Phys. Lett. A **26**, 1521 (2011) [arXiv:1103.5061 [hep-ph]]; M. Farina, M. Kadastik, D. Pappadopulo, J. Pata, M. Raidal and A. Strumia, Nucl. Phys. B **853**, 607 (2011) [arXiv:1104.3572 [hep-ph]]; S. Profumo, Phys. Rev. D **84**, 015008 (2011) [arXiv:1105.5162 [hep-ph]]; T. Li, J. A. Maxin, D. V. Nanopoulos and J. W. Walker, arXiv:1106.1165 [hep-ph]; N. Bhattacharyya, A. Choudhury and A. Datta, Phys. Rev. D **84**, 095006 (2011) [arXiv:1107.1997 [hep-ph]]; A. Fowlie, A. Kalinowski, M. Kazana, L. Roszkowski and Y. L. S. Tsai, arXiv:1111.6098 [hep-ph].
- [47] G. Aad *et al.* [ATLAS Collaboration], arXiv:1109.6572 [hep-ex].
- [48] ATLAS Collaboration,
<http://cdsweb.cern.ch/record/1383835/files/ATLAS-CONF-2011-132.pdf>.
- [49] S. Chatrchyan *et al.* [CMS Collaboration], arXiv:1109.2352 [hep-ex].
- [50] CMS Collaboration,
<http://cdsweb.cern.ch/record/1378096/files/HIG-11-020-pas.pdf>.
- [51] S. Chatrchyan *et al.* [CMS Collaboration], arXiv:1107.5834 [hep-ex].
- [52] R. Aaij *et al.* [LHCb Collaboration], Phys. Lett. B **699** (2011) 330 [arXiv:1103.2465 [hep-ex]].
- [53] A. Bottino, F. Donato, N. Fornengo and S. Scopel, Astropart. Phys. **13** (2000) 215 [arXiv:hep-ph/9909228]; E. Accomando, R. L. Arnowitt, B. Dutta and Y. Santoso, Nucl. Phys. B **585** (2000) 124 [arXiv:hep-ph/0001019]; J. R. Ellis, K. A. Olive, Y. Santoso and V. C. Spanos, Phys. Rev. D **71** (2005) 095007 [arXiv:hep-ph/0502001]; J. R. Ellis, K. A. Olive and C. Savage, Phys. Rev. D **77** (2008) 065026 [arXiv:0801.3656 [hep-ph]]; J. Gasser, H. Leutwyler and M. E. Sainio, Phys. Lett. B **253** (1991) 252; M. Knecht, PiN Newslett. **15** (1999) 108 [arXiv:hep-ph/9912443]; M. E. Sainio, PiN Newslett. **16** (2002) 138 [arXiv:hep-ph/0110413]; B. Borasoy and U. G. Meissner, Annals Phys. **254** (1997) 192 [arXiv:hep-ph/9607432]; M. M. Pavan, I. I. Strakovsky, R. L. Workman and R. A. Arndt, PiN Newslett. **16** (2002) 110 [arXiv:hep-ph/0111066]; see also T. Strauch *et al.*, arXiv:1011.2415 [nucl-ex], as interpreted in V. Baru, C. Hanhart, M. Hoferichter, B. Kubis, A. Nogga and D. R. Phillips, arXiv:1003.4444 [nucl-th].
- [54] The ATLAS and CMS Collaborations,
<https://cdsweb.cern.ch/record/1399607/files/HIG-11-023-pas.pdf>.
- [55] CMS Collaboration,
<http://cdsweb.cern.ch/record/1406347/files/HIG-11-032-pas.pdf>; ATLAS Collaboration,
<http://cdsweb.cern.ch/record/1406358/files/ATLAS-CONF-2011-163.pdf>.
- [56] S. Schael *et al.* [ALEPH, DELPHI, L3, OPAL Collaborations and LEP Working Group for Higgs boson searches], Eur. Phys. J. C **47** (2006) 547 [arXiv:hep-ex/0602042].
- [57] <http://tevnpnphwg.fnal.gov/> and references therein.
- [58] O. Buchmueller, R. Cavanaugh, A. De Roeck, M. J. Dolan, J. R. Ellis, H. Flacher, S. Heinemeyer and G. Isidori *et al.*, arXiv:1112.3564 [hep-ph].
- [59] H. Baer, V. Barger and A. Mustafayev, arXiv:1112.3017 [hep-ph]; J. L. Feng, K. T. Matchev and D. Sanford, arXiv:1112.3021 [hep-ph]; S. Heinemeyer, O. Stal and G. Weiglein, arXiv:1112.3026 [hep-ph]; A. Arbey, M. Battaglia, A. Djouadi, F. Mahmoudi and J. Quevillon, arXiv:1112.3028 [hep-ph]; P. Draper, P. Meade, M. Reece and D. Shih, arXiv:1112.3068 [hep-ph]; M. Kadastik, K. Kannike, A. Racioppi and M. Raidal, arXiv:1112.3647 [hep-ph]; N. Karagiannakis, G. Lazarides and C. Pallis, arXiv:1201.2111 [hep-ph].